RESEARCH ARTICLE





Check for updates

Potential energy surfaces and dynamic properties via ab initio composite and density functional approaches

Prajay Patel 1,2 | Joseph Chung | Max Aksel Bowman | Inga Ulusoy 1,3 | Inga Ulusoy 1 Angela K. Wilson 10

Correspondence

Angela K. Wilson, Department of Chemistry, Michigan State University, East Lansing, MI,

Email: akwilson@msu.edu

Funding information

National Science Foundation, Grant/Award Numbers: CHE-1900086, CHE-2154526

Abstract

Vibrational spectroscopy enables critical insight into the structural and dynamic properties of molecules. Presently, the majority of theoretical approaches to spectroscopy employ wavefunction-based ab initio or density functional methods that rely on the harmonic approximation. This approximation breaks down for large molecules with strongly anharmonic bonds or for molecules with large internuclear separations. An alternative to these methods involves generating molecular anharmonic potential energy surfaces (potentials) and using them to extrapolate the vibrational frequencies. This study examines the efficacy of density functional theory (DFT) and the correlation consistent Composite Approach (ccCA) in generating anharmonic frequencies from potentials of small main group molecules. Vibrational self-consistent field Theory (VSCF) and post-VSCF methods were used to calculate the fundamental frequencies of these molecules from their potentials. Functional choice, basis set selection, and mode-coupling are also examined as factors in influencing accuracy. The absolute deviations for the calculated frequencies using potentials at the ccCA level of theory were lower than the potentials at the DFT level. With DFT resulting in bending modes that are better described than those of ccCA, a multilevel DFT:ccCA approach where DFT potentials are used for single vibrational mode potentials and ccCA is used for vibrational mode-mode couplings can be utilized for larger polyatomic systems. The frequencies obtained with this multilevel approach using VCIPSI-PT2 were closer to experimental frequencies than the scaled harmonic frequencies, indicating the success of utilizing post-VSCF methods to generate more accurate representations of computed infrared spectra.

KEYWORDS

anharmonic, ccCA, composite, DFT, harmonic, potential energy surface, vibrational frequencies, VSCF, VCIPSI-PT2

This is an open access article under the terms of the Creative Commons Attribution License, which permits use, distribution and reproduction in any medium, provided the original work is properly cited.

© 2024 The Authors. Journal of Computational Chemistry published by Wiley Periodicals LLC.



¹Department of Chemistry, Michigan State University, East Lansing, Michigan, USA

²Chemistry Department, University of Dallas, Irving Texas USA

³Scientific Software Center, Interdisciplinary Center for Scientific Computing, Heidelberg University, Heidelberg, Germany

1 | INTRODUCTION

Vibrational spectroscopy is one of the most useful spectroscopic techniques due to its unique window into the structure, dynamical behavior, and bonding properties of molecules. Vibrational interactions are critical to the understanding of infrared absorption, reaction mechanisms, and kinetics as well as characterizing the interstellar medium with infrared spectrographs like the Near Infrared Spectrograph (NIRSpec) on the James Webb Space Telescope. Using electronic structure methods, calculated infrared transitions derived from the Hessian can be utilized to predict thermodynamic properties like the enthalpy of formation and reaction barriers via the vibrational contributions to the molecular partition function at a given temperature.²⁻⁶ As well, computational approaches can aid in experiments where the resolution is insufficient or there are difficulties in isolating the molecule, such as for diatomics, amino acids, metalligand interactions, or even short-lived molecules like transition states in a chemical reaction or radical complexes.8 facilitating the interpretation and assignment of vibrational features. 9-14

Computational chemistry methods generally employ a harmonic approximation to predict vibrational spectra. The frequencies and other properties are then typically adjusted by a scaling factor, to provide a global and approximate route to correct for anharmonicity for low and high frequencies. While such an approach can be quite useful, an anharmonic approach can provide a more realistic description of the vibrational properties, including the overtones. Under the ever, obtaining anharmonic vibrational frequencies is far more computationally demanding than obtaining harmonic frequencies, as anharmonic frequencies require the third or fourth derivative of the energy, whereas harmonic frequencies only require the Hessian.

To achieve predictions of vibrational properties, electronic structures methods have been used to generate potential energy surfaces (PESs), from which vibrational frequencies have been obtained that are within several wavenumbers (cm⁻¹) of experiment, ^{10,22-25} enabling the identification of vibrational fingerprints, that is, a set of vibrational frequencies unique to every molecule. However, as indicated, these methods entail high computational cost (memory, disk space, and CPU time), ^{10,11} which can become particularly daunting due to the number of calculations needed to generate the grid points for the requisite PESs, easily reaching tens of thousands to a million grid points. ^{22,23} Thus, the combination of electronic structure methods with the vast number of grid points required for a PES reduces their utility for predicting vibrational properties within several cm⁻¹.

There is continual development towards more computationally efficient methods that yield vibrational frequency predictions within several cm⁻¹ from well-established, reliable experiments. Efficient processes targeting PES generation have been developed to reduce the computational cost while yielding deviations from experimental vibrations by several cm⁻¹ or deviations less than 1 kcal mol⁻¹ for reaction barriers. ^{22,26-28} The correlation consistent Composite Approach (ccCA)²⁹⁻³¹ is considered, as a route to alleviate the cost of generating PESs. For example, the multireference wavefunction ccCA (MR-ccCA) was utilized to analyze the potential energy curve of the

torsional rotation of the carbon–carbon double bond in ethylene, predicting the barrier height of cis-trans isomerism and yielded errors approximately 0.7 kcal mol⁻¹ from experiment.²⁷ As an alternative to utilizing multireference methods, completely renormalized coupled cluster (CR-CC(2,3)) was implemented within the ccCA formalism, CR-ccCA(2,3).²⁸ This method utilizes a single reference completely renormalized coupled cluster that can correctly treat reaction pathways such as the thermal pericyclic rearrangement of bicyclo[1.1.0]butane to trans-buta-1,3-diene and chemical species, for example, diradicals, that would normally require multireference methods.

In addition to ccCA, density functional theory (DFT) can be used at a lower computational cost relative to the *ab initio* methods utilized for vibrational spectroscopy. ¹⁶ Density functionals have been largely designed for main group thermochemical properties; however, DFT cannot adequately describe noncovalent interactions, such as π - π stacking or weak hydrogen bonding, crucial in larger polyatomic molecules without empirical corrections like dispersion and could be significant when describing weakly-bound ligands and noncovalent interactions between two molecules. ^{32,33}

To account for anharmonicity computationally, strategies often include a perturbative correction, such as VPT2, to the potential. Theories like the local vibrational mode theory developed by Konkoli and Cremer^{34–37} utilizes mass-decoupled Euler-Lagrange equations to do local model analysis (LMA) and the characterization of the normal modes (CNM), which leads to a descriptor of the bond strength accounting for various bonding interactions such as noncovalent interactions, hydrogen bonds, and halogen bonds. 38-40 For example, in a study by Quintano et al., 40 the fingerprint normal vibrational modes of the base pairs of DNA were quantified prior to and upon base pairing at the ωB97X-D/aug-ccpVTZ level of theory using water as an implicit solvent. Their analysis showed how the interactions between C=C and C=O bonds in nucleobases does not significantly affect the C=C bond lengths or related structural and electronic density-based properties of the base pairs upon pairing. Alternative methods for analyzing anharmonic corrections for vibrational spectroscopy include using quartic force fields combined with vibrational perturbation theory 41,42 and re-parameterized semiempirical methods⁴³ targeting molecules relevant in astrochemistry.⁴²⁻⁴⁵

While local vibrational model theory is a powerful theory to describe CNM, vibrational self-consistent field (VSCF) theory, which was developed in the late 1970s, fully accounts for anharmonicity by considering the vibrational Schrödinger Equation. Approximations are made that make VSCF theory analogous to Hartree-Fock theory. 46-50 Studies implement VSCF theory on certain biologically pertinent vibrations for amino acid peptide chains, 22,51 which are not typically targeted with the rigorous ab initio methods utilized for potential energy surfaces (PESs) of diatomics and small polyatomic molecules like H₂O and formaldehyde. ^{23,52,53} In a study by Roy et al., ²² a VSCF-PT2 approach was utilized with both a B3LYP-D2 potential and a multilevel HF/MP2 potential to characterize anharmonic vibrational motion of an opioid peptide [Ala², Leu⁵]-leucine enkephalin (ALE). They found that the B3LYP and multilevel HF/MP2 potential systematically underestimated and overestimated the experimental frequencies for the OH and NH stretching modes for each amino acid,

respectively, by a few tens of cm⁻¹. The average of the frequencies compensates for the respective under and overestimation of frequencies and yielded theoretical predictions within 10 cm⁻¹ of experiment, which was better than the B3LYP and the multilevel HF/MP2 potentials individually as well as scaled harmonic calculations, thus showing the efficacy of VSCF theory towards predicting anharmonic vibrations for systems as large as a pentapeptide.

In this work, ccCA and DFT have been used to generate PESs for diatomic and small polyatomic molecules to predict structural and vibrational properties such as frequencies and infrared absorbance intensities in tandem with vibrational self-consistent field (VSCF) and post-VSCF theory. The combination of electronic structure methods such as ccCA and DFT with post-VSCF theory aims to reduce the computational cost associated with generating accurate PESs for anharmonic mode-mode couplings as well as calculating contributions from anharmonic corrections to the potential.

2 | COMPUTATIONAL METHODS

The PVSCF program^{26,54} was used for vibrational analysis and ORCA 4.0 was used for the electronic structure calculations necessary to generate potential energy surfaces (PESs). 55,56 The molecule set included 20 molecules: H₂, CO, LiH, N₂, NO⁺, OH, NH, HF, BF, O₂, SiO, H₂O, CO₂, NH₃, C₂H₂, C₂H₄, C₂H₆, cis-3-aminophenol, and trans-3-aminophenol. These were chosen based on the availability of experimental data on the frequencies of these molecules as well as other post-HF methods for predicting anharmonic frequencies. 33 Experimental vibrational frequencies were obtained from Herzberg, Huber, and Shimanouchi. 57-59 Equilibrium bond lengths for diatomic molecules were obtained from CISD/cc-pVTZ calculations to locate the starting point for generating the potential using an ab initio non-perturbative method and the initial Hessians were generated using RI-B3LYP-D3/aug-cc-pVTZ within the ORCA package. Since the PVSCF program uses the Hessian as an initial guess, a Hessian generated with a more approximate method is sufficient for the purpose of this study. For polyatomic molecules, B3LYP/cc-pVTZ geometries and hessians were used since optimized geometries and the zero-point vibrational energy are obtained at the B3LYP/cc-pVTZ level of theory as part of the ccCA methodology.30

The potentials are generated via an interpolation of 16 grid points selected by PVSCF by a multimode expansion using curvilinear coordinates. Curvilinear coordinates are a nonlinear function of Cartesian coordinates where the coordinate lines are curved to follow the normal mode vectors. This allows for a more robust description of vibrational motion. Potential energy curves (PECs) are generated for diatomics while PESs that visualize the effect of two different vibrational modes concurrently vibrating, or vibrational mode coupling, are generated for polyatomic molecules. The extracted potential energies and dipole moments are then run with the PVSCF program to obtain the anharmonic frequencies and infrared (IR) intensities of each molecule, respectively. For diatomic molecules, a Fourier Grid Hamiltonian approach is used to calculate the single vibrational frequency. 61,62 For all polyatomic molecules, a vibrational configuration

interaction method (VCIPSI-PT2) is used to analyze the effects of vibrational mode coupling.⁶³ VCIPSI-PT2 utilizes vibrational configuration interaction with perturbatively selected interactions (VCIPSI), which reduces the computational cost compared to standard VCI approaches while maintaining roughly the same level of accuracy.^{26,63}

2.1 | DFT methodology

Density functionals come in numerous flavors based on the number of parameters and the operations performed on the electronic density surface to varying degrees of success. For example, B3LYP^{64,65} is heavily parameterized for main group thermochemistry while TPSS⁶⁶ has no empirical parameters; yet both density functionals are popular and yield low mean absolute errors for main group thermochemistry.⁶⁷ For spectroscopic purposes, these functionals provide an avenue to examine other cost-effective methods for predicting anharmonic vibrational frequencies and the effect of parameterization of a functional on spectroscopic properties. Therefore, TPSS and B3LYP were used as the density functionals in this work.

Dunning's standard and augmented correlation consistent basis sets from double- to quintuple-ζ (cc-pVnZ (VnZ) and aug-cc-pVnZ (aVnZ), n = D, T, Q, 5) were used.⁶⁸ These basis sets were built to systematically increase the types of functions included in the basis set, which leads to a smooth convergence towards an infinite basis set that would describe all possible space in which electrons exist. The energy associated with an infinite basis set, or the complete basis set (CBS) limit, is an extrapolated estimate of the results from the finite basis sets used. With DFT, the standard CBS extrapolation formulas may not be applicable as DFT may not behave variationally with respect to increasing the basis set quality, that is, the Kohn-Sham energy may not monotonically decrease or increase as a function of the ζ -level of the basis set. Points that do not follow a monotonic trend were screened out for extrapolating to the Kohn-Sham limit. One such extrapolation scheme to extrapolate to the Kohn-Sham limit, which is analogous to the CBS limit for wavefunction-based methods, investigated in this work for DFT methods is the three-point Feller extrapolation scheme.⁶⁹ The Feller three-point extrapolation scheme (Equation 1) was used since this scheme allows the extrapolation function to converge to a limit closer to the electronic energy that corresponds to experimental values for thermodynamic properties like enthalpies of formation, and uses the exponential form

$$E(n) = E_{\infty} + Ae^{-Bn}, \tag{1}$$

where, E(n) is the energy value from the basis set, n is equal to the cardinal number of the basis set, and E_{∞} stands for the basis set limit (Kohn-Sham limit or CBS limit). A and B are fitting parameters. The effects of the Feller extrapolation scheme were examined to provide insight into energies that would be obtained when using a more computationally demanding basis set (such as $6-\zeta$ or higher). For polyatomic molecules with more than three atoms, only cc-pVTZ and augcc-pVTZ was used.

2.2 | ccCA methodology

The implementation of ccCA has been described in previous work. As a quick overview, the HF energies are extrapolated to the CBS limit using Equation (1) with B set to 1.63 from a study by Halkier et al. 70,71 The MP2 energies are extrapolated to the CBS limit with the Peterson (P) (Equation 2), Schwartz-3 (S3) (Equation 3), Schwartz-4 (S4) (Equation 4), and an average of the Peterson and Schwartz-3 extrapolation schemes. $^{72-74}$

$$E(n) = E_{\infty} + Be^{-(n-1)} + Ce^{-(n-1)^2},$$
 (2)

$$E(I_{max}) = E_{\infty} + \frac{B}{(I_{max})^3},$$
(3)

$$E(I_{max}) = E_{\infty} + \frac{B}{(I_{max} + \frac{1}{2})^4},$$
 (4)

where, E_{∞} represents the CBS limit and B and C are fitting parameters (Equation 2), and I_{max} is the highest angular momentum function in the basis set (Equations 3 and 4). Corrections including the effects of core-core correlation, core-valence correlation, and scalar relativity, are included in the total ccCA energy. The zero-point vibrational energy is not included as the goal is to generate a potential energy surface for vibrational calculations.

Standard Cartesian, or rectilinear, coordinates were used for diatomics and linear polyatomic molecules (CO₂, C₂H₂). Curvilinear coordinates were used for nonlinear polyatomic molecules (H₂O, aminophenol isomers). SCF energies were converged to 10^{-8} E_h in all single point energy calculations. ^{29,30} ccCA electronic energies were used to generate all potential energy curves for singular vibrational motion and surfaces for mode-mode coupling, that is, simultaneous vibrational motion for two vibrational modes.

For C_2H_4 , C_2H_6 , and aminophenol isomers, DFT calculations were used to generate all vibrational mode couplings, for example, all 324 vibrational mode couplings for C_2H_6 . Since the coupling strength is largely independent of the choice of method used to generate the PES, the number of vibrational mode couplings were decreased via a screening threshold to isolate strongly coupled vibrational modes. 15,60 The PESs of the screened vibrational mode couplings were then calculated via DFT or higher level of theory like ccCA. In this work, this approach to generate the PES of only the screened strongly coupled modes is denoted as the FASTVCI approach. Selected vibrational modes from coupling maps are provided in Supplemental Information.

3 | RESULTS AND DISCUSSIONS

The calculated frequencies for diatomics molecules are provided in Tables S1–S3 and calculated frequencies for polyatomics are listed in Tables S4–S8. The mean absolute deviation (MAD) was analyzed by basis set, functional, and by number of atoms to note specific trends or certain occurrences within the calculations. For ccCA potentials, utilizing different extrapolation schemes did not significantly affect the predicted vibrational frequency as shown in Table S1. Therefore, for conciseness, only the frequencies predicted with ccCA-S4 potentials are presented as ccCA-S4 yielded the lowest errors of all extrapolation schemes utilized.

3.1 | Diatomics

With DFT potentials at the complete basis set limit, the calculated frequencies yielded absolute deviations that ranged from 0 to 149 cm⁻¹ depending on the molecule and functional whereas with ccCA potentials, the calculated frequencies yielded absolute deviations that ranged from 0 to 22 cm⁻¹. Figure 1 shows the absolute deviations from

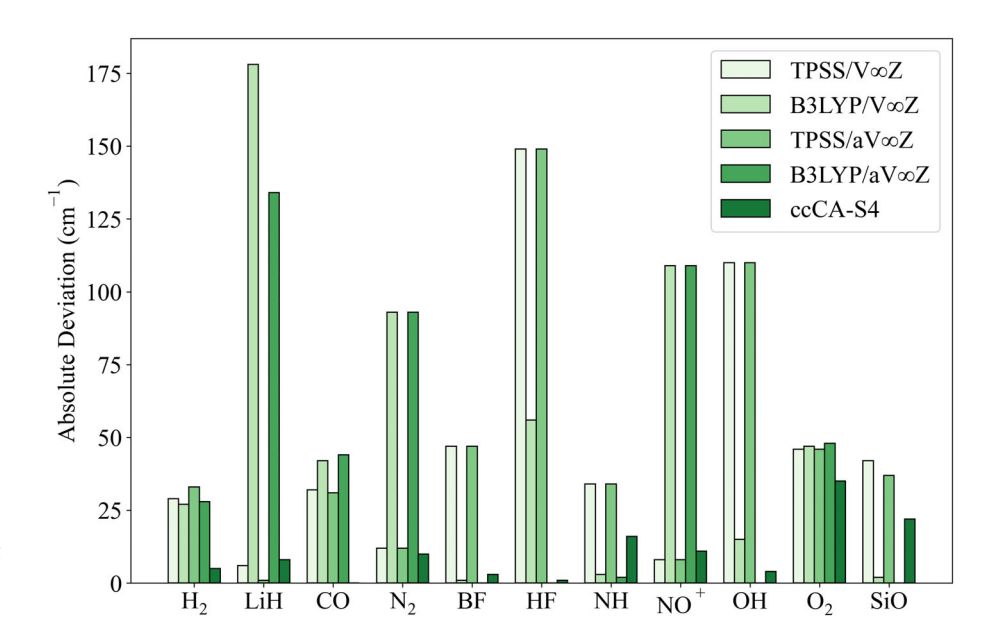


FIGURE 1 Absolute deviation of vibrational frequencies for diatomics using TPSS/V∞Z, B3LYP/V∞Z, TPSS/aV∞Z, B3LYP/aV∞Z, and ccCA-S4.

experimental vibrational frequencies with the potential energy curves (PECs) generated at the indicated level of theory, that is, DFT/V $_{\infty}$ Z or ccCA. Examining functional choice, frequencies predicted with B3LYP-generated potential energy curves (PECs) for H $_2$, BF, HF, NH, OH, O $_2$, and SiO yielded smaller absolute deviations compared to TPSS PECs as shown in Figure 1, which implies that TPSS yielded lower absolute deviations for LiH, CO, N $_2$, and NO $^+$. For N $_2$, the predicted frequency generated with TPSS aligned with those predicted with ccCA-S4. Based on the choice of molecule, functional choice had a larger effect on predicted vibrational frequency than basis set choice.

Using DFT in combination with the augmented correlation consistent basis sets tended to produce lower MADs for experimental frequencies in comparison to using DFT with the standard correlation consistent basis sets. For B3LYP/VnZ and B3LYP/aVnZ, the MAD decreased from 43 ± 37 to 39 ± 35 cm⁻¹, respectively, and 57 ± 52 to $55 \pm 50 \text{ cm}^{-1}$ for TPSS/VnZ and TPSS/aVnZ, respectively, for the set of diatomics. While these results are statistically indifferent verified through unpaired two-tailed t tests. Figure 1 shows how using aV∞Z lowers the deviations for LiH, HF, and OH by up to 50 cm⁻¹ in comparison to the increase in deviation by 4 cm⁻¹ for H₂. When comparing the effect of basis set quality, all frequencies calculated using the DFT/VTZ, DFT/VQZ, and DFT/V5Z potentials were statistically indifferent from each other verified through unpaired two-tailed t tests (see SI for calculated frequencies at each level of theory). Therefore, triple-ζ quality basis sets may be useful as a compromise between cost and accuracy for generating potentials describing vibrational motion for polyatomic molecules.

Across all diatomics examined, ccCA yielded a MAD of $9 \pm 7 \text{ cm}^{-1}$ whereas B3LYP/VnZ and TPSS/VnZ yielded MADs of 43 \pm 37 and 57 \pm 52 cm⁻¹, respectively (Figure 1). This indicates that using potentials generated with ccCA yield lower deviations for predicted frequencies than DFT, with the notable exception of SiO, where using B3LYP regardless of basis set yielded frequencies closer to experiment than ccCA by approximately 20 cm⁻¹. With ccCA, diatomics that have a larger difference in mass between the two atoms and larger dipole moments (OH, BF, and HF) tended to yield lower deviations from experiment for calculated frequencies with the exception of NH, which yielded an error of 16 cm⁻¹. PECs for homonuclear diatomics yielded higher deviations with an increase in mass as H_2 , N_2 , and O_2 , yielded errors of 5, 10, and 11 cm⁻¹, respectively. As well, PECs for LiH and NO+, heteronuclear diatomics with similar mass and smaller dipole moments between the two atoms, tended to yield higher errors (8 and 11 cm⁻¹) among the ccCA results although PECs for CO and BF yielded errors of 0 and 2 cm⁻¹, respectively. This

would suggest that unlike DFT, there is no consistent trend between the atomic masses and the frequencies generated with ccCA PECs even though PECs at the ccCA level of theory generates lower errors across all diatomics compared to DFT PECs.

The relative CPU time was measured for a few diatomics to show the approximate cost of generating a PEC of 17 grid points with DFT, ccCA, and CCSD(T,full)/aug-cc-pCV5Z where full denotes the inclusion of all electrons for first-row main group diatomics in the correlation space (Table 1). As expected, B3LYP calculations are more computationally affordable than ab initio methods but yielded higher deviations for the molecules used (Table 2). Also, generating a PEC at the ccCA level, which aims to model energies at the CCSD(T,full)/ aug-cc-pCV∞Z-DK level, is more affordable than using CCSD(T,full)/ aug-cc-pCV5Z by several hours depending on the molecule size. As shown in Table 1 for example, ccCA yielded a percent CPU time savings of 99.16% for N2 relative to CCSD(T,full)/aug-cc-pCV5Z. Interestingly, the use of CCSD(T,full)/aug-cc-pCV5Z to generate the PES yielded larger absolute errors (10 \pm 3 cm⁻¹) than ccCA (6 \pm 4 cm⁻¹) for these molecules. The main cause was that for CO, the ccCA and CCSD(T,full)/aug-cc-pCV5Z potential yielded errors of 0 and 15 cm⁻¹, respectively, for the calculated fundamental frequency. The higher absolute errors and large increase in CPU time between CCSD(T,full)/ aug-cc-pCV5Z and ccCA suggests that potentials generated with ccCA are more accurate when using a VSCF approach.

3.2 | H₂O, CO₂, and NH₃

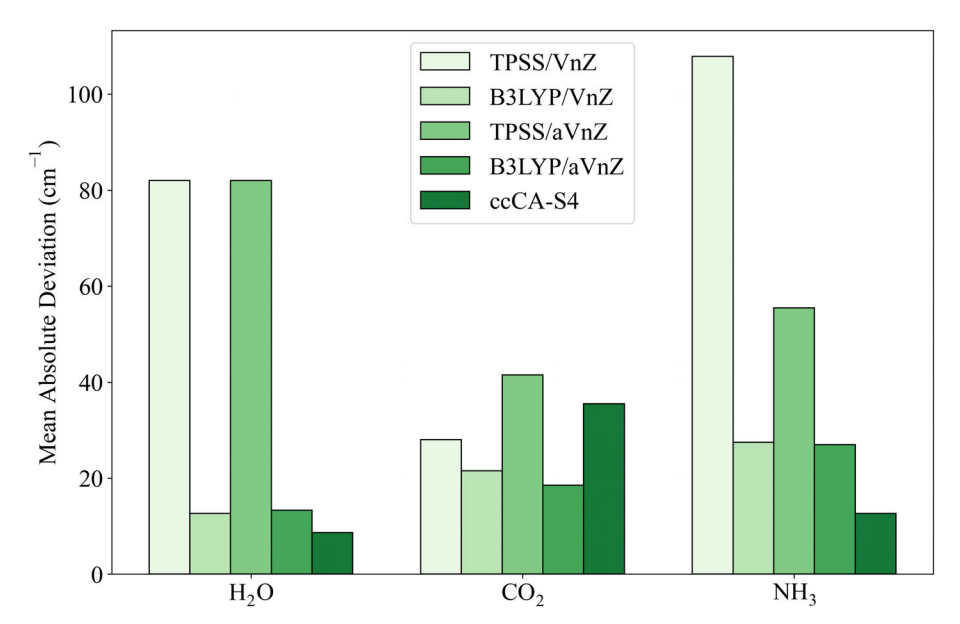
For DFT potentials, both functional choice and basis set quality affected the accuracy of predicted frequencies and the type of vibration that is observed, that is, stretching, bending, or inversion. For ccCA, the range in deviation is primarily due to the type of vibration observed. In Figure 2, the DFT potentials are obtained at the Kohn-Sham limit ($V \infty Z$ and $aV \infty Z$) for H_2O and CO_2 since there are

TABLE 1 Percent CPU time used relative to CCSD(T,full)/aug-cc-pCV5Z to generate all 17 grid points of the PEC for select diatomics.

	B3LYP/aVTZ	ccCA
H ₂	1.19	9.34
LiH	0.11	1.18
CO	0.03	0.99
N_2	0.02	0.84

	B3LYP/aVTZ	ccCA	CCSD(T,full)/aug-cc-pCV5Z	Ехр
H ₂	4189	4157	4155	4162.2
LiH	1372	1368	1348	1360
СО	2186	2143	2128	2143
N_2	2420	2340	2323	2330
MAD ± STD	43 ± 29	6 ± 4	10 ± 3	

TABLE 2 Calculated frequencies in cm⁻¹ for B3LYP/aVTZ, ccCA, and CCSD (T,full)/aug-cc-pCV5Z for diatomics in Table 1.



only 3 and 4 vibrational normal modes (3 and 7 vibrational mode-mode couplings, or the PES describing two vibrations occurring simultaneously), respectively. H_2O , CO_2 , and NH_3 yielded a larger range of deviations from experimental frequencies than the diatomics, wavering from 2 to 294 cm⁻¹ with DFT potentials and from 2 to 57 cm⁻¹ for ccCA potentials. For NH_3 , the vibrational mode-mode coupling potentials were generated at the triple- ζ level based on the results for the diatomic molecules, small polyatomic molecules, for example, H_2O and CO_2 , and the number of vibrational mode-mode coupling potentials required for six normal modes. All vibrational mode-mode coupling potentials consist of 256 grid points.

In Figure 2, the MAD is the average across all frequencies per molecule for each method (B3LYP/VnZ, B3LYP/aVnZ, TPSS/VnZ, TPSS/aVnZ, and ccCA). For DFT, the choice between aVnZ and VnZ altered the curvature of the potentials enough to yield larger variations in the errors for calculated frequencies between the molecules except for H₂O. When aVnZ was used in H₂O, the error across all vibrations was the same as $V \infty Z$, regardless of functional choice. This indicates that when using DFT to generate potentials for vibrational calculations, augmented basis sets properly characterize both bending and stretching behavior for small polyatomic species.

Functional choice was a larger factor in terms of general curvature of the potentials as B3LYP-generated potentials yielded deviations for calculated frequency approximately 20–60 cm $^{-1}$ lower than TPSS-generated potentials. For $\rm H_2O$, $\rm CO_2$, and $\rm NH_3$, TPSS potentials inadequately described both symmetric and asymmetric stretching modes with errors ranging from 70 to 225 cm $^{-1}$, whereas B3LYP potentials yielded errors in the range of 3–55 cm $^{-1}$. In comparison, the bending vibrational modes yielded errors ranging from 19 to 42 cm $^{-1}$ for TPSS potentials.

With ccCA, the stretching modes for H_2O yielded deviations within 2 cm⁻¹ of experiment, whereas the calculated bending mode was $\sim \! 20 \text{ cm}^{-1}$ larger than the experimental frequency. The difference of 20 cm^{-1} is most likely due to the weak coupling between

the bending and stretching modes and may be corrected through coupling all three vibrational modes together simultaneously. For CO_2 , ccCA potentials did not properly characterize the vibrational motion of the out-of-plane bending, and stretching normal modes with deviation of 40, 37, and 56 cm⁻¹, respectively. This may be in part due to the use of a standard Cartesian coordinate system for displacing the molecule in vibration whereas the deviations are generally lower when using a curvilinear coordinate system as is the case for H_2O .

For NH₃, ccCA potentials utilized for VCIPSI-PT2 predicted the vibrational motion corresponding to NH₃ inversion to within 10 cm^{-1} and N—H stretching modes within 15 cm^{-1} . The pyramidal inversion vibration creates a symmetry change from C_{3v} to the D_{3h} point groups and is characterized by a small reaction barrier ($\sim 5 \text{ kcal mol}^{-1}$). This analysis indicates that when using a curvilinear coordinate system, ccCA potentials yield lower errors for stretching modes opposed to bending modes, such as for H_2O .

When considering the single mode potential energy curves for H₂O and CO₂, the O—H symmetric stretching potential for ccCA more closely resembles the potential generated with B3LYP whereas the C-O symmetric stretching potential for ccCA energetically lies in between the potentials generated with B3LYP and TPSS (Figure 3), which explains the observed trend of the MADs for all vibrational motions with respect to the smaller polyatomic molecules. The other single mode potentials for the asymmetric stretching and bending motions for both H₂O and CO₂ were very similar in shape. For H₂O, CO₂, and NH₃, the DFT potentials for the symmetric stretches were the largest contributor to their performance in terms of lower deviations from experimental frequencies. In hybrid functionals, varying the percentage of exact exchange derived from the Hartree-Fock method using Kohn-Sham orbitals have been shown to affect the magnitude of both thermodynamic and spectroscopic properties, for example, the pK_a⁷⁵ and the pre-edge energy in X-ray Absorption Spectroscopy, 76 respectively, indicating that the

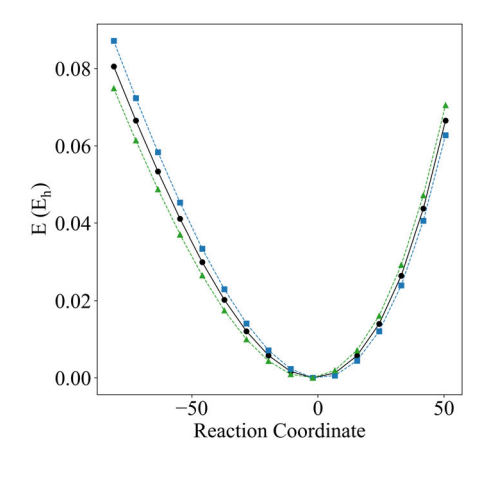


FIGURE 3 The single mode potential energy curves for the O—H symmetric stretch in H_2O (left) and the C—O symmetric stretch in CO_2 (right) with ccCA, B3LYP/V ∞ Z, and TPSS/V ∞ Z.

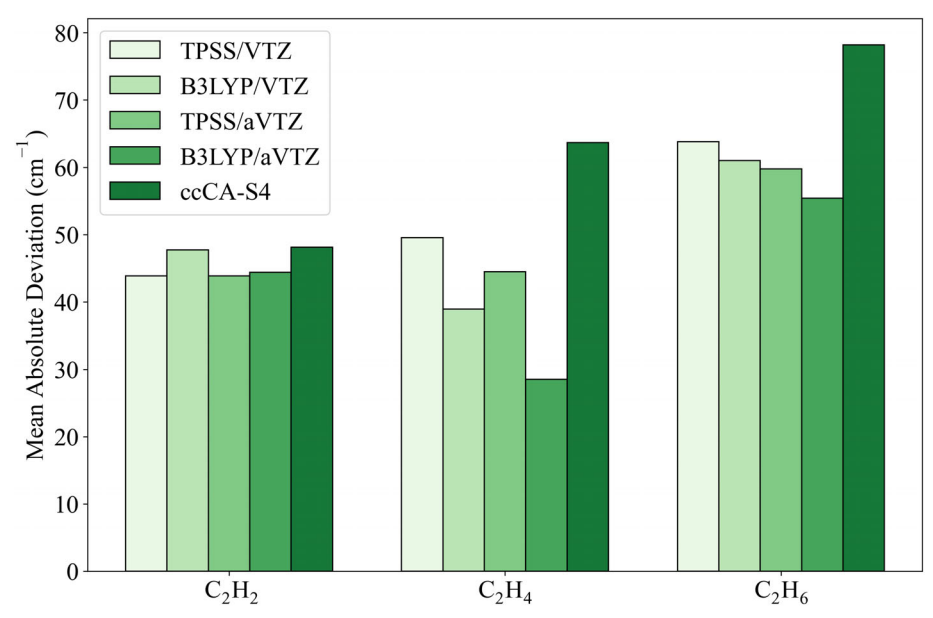


FIGURE 4 Mean absolute deviation of vibrational frequencies for C₂H₂, C₂H₄, and C₂H₆ using TPSS/VTZ, B3LYP/VTZ, TPSS/aVTZ, B3LYP/aVTZ, and ccCA-S4.

exact exchange parameter within B3LYP is a larger contributor to the predicted curvature of the single mode potential energy curves than the empirical parameterization of a functional and the local kinetic energy effects. Therefore, hybrid DFT functionals are better candidates than local DFT functionals for generating potentials similar to potentials generated via ccCA.

3.3 | Hydrocarbons

PESs for C_2H_2 , C_2H_4 , and C_2H_6 were generated with basis set superposition error (BSSE)-corrected energies. With ccCA, only strongly coupled vibrational modes, which are depicted within mode-mode coupling maps (see SI), are considered for C_2H_4 and C_2H_6 . By removing non-essential vibrational coupling elements from the potential, a FASTVCI approach is attained. By utilizing this approach, the computational time to generate all vibrational potential energy surfaces for ethene is reduced by approximately a factor of 6 (12 out of 78 coupling modes for C_2H_4 were calculated with ccCA) for ethene as only the potential energy surfaces for all the strongly coupled vibrational

modes (shown as shaded squares in Figure S1) were generated with ccCA. For ethene, vibrational modes 9–12 characterize the C—H stretching modes (both symmetric and asymmetric). In general, symmetric and asymmetric vibrations are strongly coupled largely due to the effect each type of vibration has on the other.

In contrast to C_2H_4 , which exhibited stronger coupling modes for the C—H stretches at approximately 3000 cm $^{-1}$, C_2H_6 only had one strong coupling mode in this region, which is the coupling between C—H symmetric and C—H asymmetric stretches. Other modes that were strongly coupled include the rotational barrier of C_2H_6 around the C—C bond and C—C stretching. Including the coupling strength screened out 67 vibrational mode-mode couplings, leaving 11. This effectively reduced the computational cost of generating the full 2D surface by approximately 93%.

For the hydrocarbons, there is a noticeable improvement among frequencies predicted with DFT potentials relative to ccCA potentials (Figure 4). TPSS provided a smaller absolute deviation in ethyne, while B3LYP was preferred for ethene and ethane. The results for the hydrocarbons are consistent when comparing the basis set and molecule choice in that DFT/aVTZ potentials yielded lower errors for

calculated frequencies relative to using DFT/VTZ potentials when using VCIPSI-PT2 to compute the frequencies.

BSSE-corrections were necessary for the PESs of the hydrocarbons since the simultaneous torsional and stretching motions of the C—H and C—C bonds caused an additional lowering in the calculated potential energy when not counterpoise-corrected, which in turn increased the mode-mode coupling strength and affected the convergence behavior of the VCIPSI-PT2 calculations. As an effect of BSSE on the potentials, the deviations from experimental frequencies with the ccCA potentials monotonically increased as a function of the number of C-H bonds from C_2H_2 to C_2H_6 . For the noncounterpoise-corrected potentials, this resulted in most of the modemode couplings involving a C-H stretching motion to have a high coupling strength, and generally increased the coupling strength of torsional-torsional vibrational couplings. When corrected for BSSE, the C-H stretching modes are no longer highly coupled to all torsional motions within C₂H₂, C₂H₄, and C₂H₆. For example, in C₂H₆, only the coupling between C-H symmetric and C-H asymmetric stretches was strongly coupled in addition to a few of the rotational and torsional motions.

Considering all observed frequencies, DFT potentials yield lower MADs from experimental frequencies than ccCA. For C₂H₂, the difference in magnitude between total MADs of frequencies predicted with DFT and ccCA potentials was approximately 5 cm⁻¹. Yet for C₂H₄ and C₂H₆, this difference increases to 10-15 cm⁻¹ primarily due to the large deviations in the C-H stretching vibrations around 3000 cm⁻¹ for ccCA potentials as well as the number of strongly coupled vibrational modes that include a non-IR active symmetric C—H stretching mode used for the FASTVCI approach. The observation of larger deviations in the C—H stretching vibrations is also consistent with other composite strategies that utilize perturbative anharmonic corrections,⁷⁷ which suggests that for molecules like C₂H₄ and C₂H₆, a softer potential as generated via DFT for the non-IR active symmetric stretches is more characteristic of the vibrational motion as shown in Figure 5. Figure 5 illustrates the ccCA and TPSS potential for the non-IR active symmetric C-H stretching mode and an IR-active C—H stretching vibration.

With ccCA potentials, the C—C stretching mode for C_2H_2 , C_2H_4 , and C_2H_6 yielded errors for predicted frequencies with VCIPSI-PT2 of 17, 21, and 7 cm⁻¹, respectively, all of which are IR inactive. This would suggest that ccCA potentials are more adequate for describing vibrations involving covalent single bonds than double or triple bonds. This is also supported in part by the low deviations observed for H_2O and NH_3 and high deviations for CO_2 observed for stretching modes.

To correct for this discrepancy between frequencies generated with DFT potentials and ccCA potentials, a multilevel approach can be utilized where the coupling elements from ccCA potentials can be added to the frequencies generated via the uncoupled DFT potentials for each vibration. This is denoted as DFT:ccCA in this work. To illustrate this concept for ethene, where the shape of the single mode PECs for both the individual non-IR active C—C and C—H symmetric stretches differ between ccCA and DFT (Figure S3), the frequencies are obtained where the mode-mode coupling elements from ccCA potentials are applied to the single mode PECs generated with TPSS/VTZ. As shown in Table 3, when using TPSS single mode PECs in tandem with ccCA mode-mode coupling potentials, the error decreases to 24 cm⁻¹ from 57 cm⁻¹ when using ccCA single mode and mode-mode coupling PECs and potentials, respectively.

While the difference between using TPSS and ccCA mode-mode coupling potentials with single mode PECs was only 1 cm⁻¹, ccCA mode-mode coupling potentials lowered the predicted frequency relative to using TPSS mode-mode coupling potentials, which lowered the deviation as TPSS potentials overestimated the C—H stretching modes (modes 9–12 in Table 3). Overall, a multilevel approach may be useful when one method generates a single mode PEC more representative of the vibrational motion indicated by the predicted frequency and for larger polyatomic systems.

3.4 | Aminophenol

For cis-3-aminophenol and trans-3-aminophenol, the NH_2 torsion, 318.5 and 329 cm⁻¹, respectively, and OH wagging vibrations, 307 and 316 cm⁻¹, respectively were examined.⁹ Each chosen

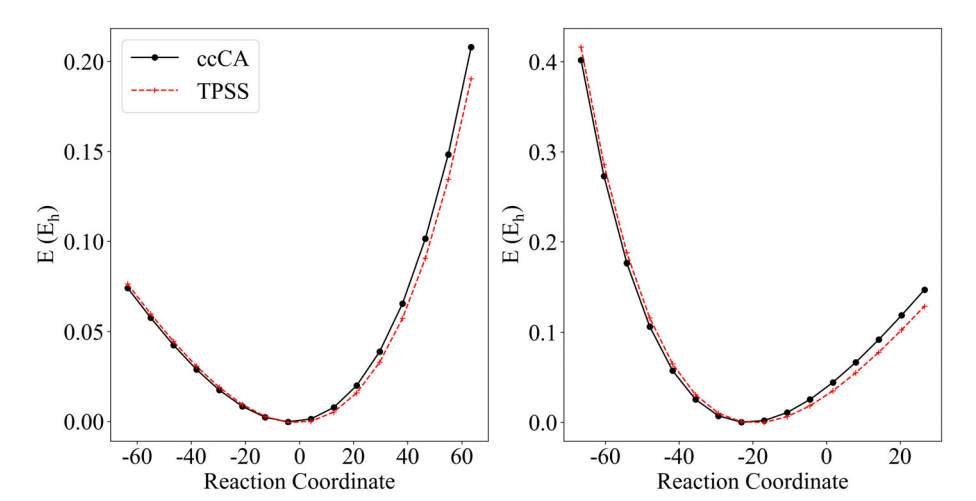


FIGURE 5 The single mode potential energy curves for the C—C symmetric stretch (left) and C—H symmetric stretch (right) of ethene generated with ccCA and TPSS/VTZ.

		TPSS:TPSS	TPSS:TPSS	ccCA-S4:ccCA-S4	TPSS:ccCA-S4
Mode	Ехр	All	FASTVCI	FASTVCI	FASTVCI
1	826	821	827	834	827
2	949	976	988	975	991
3	943	963	981	979	977
4	1023	1046	-	-	-
5	1236	1229	1238	1233	1239
6	1342	1354	1363	1360	1363
7	1444	1455	1468	1462	1467
8	1623	1628	1636	1649	1652
9	2989	3030	3050	3143	3043
10	3026	2992	3004	3104	2998
11	3103	3087	3113	3221	3105
12	3106	3118	3145	3247	3132
MAD		18	25	57	24

TABLE 3 VCIPSI-PT2 frequencies for ethene using a combination of TPSS and ccCA for single mode and vibrational mode-mode coupling potentials.

Note: The use of PECs/PESs is denoted as single:coupled. All potentials are BSSE-corrected. Mode 4 did not strongly couple to any other vibrational mode and hence are excluded from FASTVCI calculations.

vibration was coupled to all 38 other normal modes for DFT calculations. With ccCA, only strongly coupled vibrational modes determined through the DFT calculations were included in vibrational analysis. Coupling maps depicting strongly coupled vibrational modes are included in the Supplemental Information. For cis-3-aminophenol, in terms of coupling strength, only 6 of the 78 mode-mode coupling potentials were analyzed with ccCA, again reducing the cost by approximately 92%. For trans-3-aminophenol, in terms of coupling strength, only 12 of the 78 mode-mode coupling potentials were analyzed with ccCA, reducing the cost of generating the full 2D surface by approximately 84%. These vibrations were chosen since these had distinct vibrational features that separated from the IR spectra.

Calculated frequencies obtained with ccCA potentials yielded a lower deviation for experimental NH $_2$ torsion and OH wagging vibrational modes than frequencies obtained with DFT potentials. This is shown in Table 4. B3LYP/aVTZ yields lower deviations than TPSS/aVTZ for both the NH $_2$ torsion and OH wagging vibrational modes for both cis-3-aminophenol and trans-3-aminophenol. For ccCA potentials the NH $_2$ torsional mode was better characterized for cis-3-aminophenol with an error of 5.5 cm $^{-1}$ and the OH wagging motion was better characterized for trans-3-aminophenol with an error of 1 cm $^{-1}$. While the deviations obtained with ccCA potentials are lower than 10 cm $^{-1}$ for trans-3-aminophenol, this approach can be utilized to spectroscopically differentiate between aminophenol isomers that differ by the direction of the OH bond relative to the NH $_2$ substituent.

When using a multilevel approach for the aminophenol isomers, utilizing ccCA single mode PECs and B3LYP/aVTZ mode-mode coupling potentials (ccCA:B3LYP) for all mode-mode couplings between the NH₂ torsion and all other vibrations as well as between the OH wagging and all other vibrations (75 total mode-mode couplings) yielded lower deviations than if only ccCA mode-mode coupling potentials were used for cis-3-aminophenol for the few strongly

TABLE 4 Vibrational frequencies predicted with VCIPSI-PT2 for selected vibrations of cis-3-aminophenol and trans-3-aminophenol.

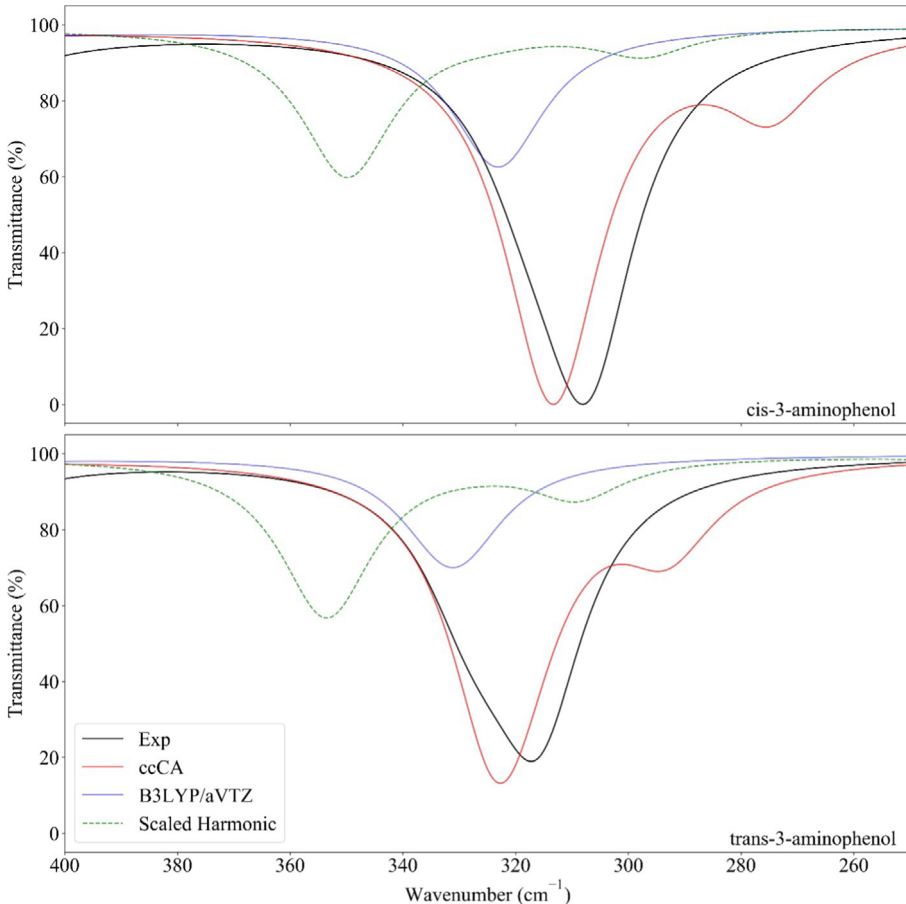
	Ехр	B3LYP/aVTZ	TPSS/aVTZ	ccCA-S4	
cis-3-aminophenol					
NH_2 torsion	318.5	322	345	313	
OH wag	307	300	296	275	
trans-3-aminophenol					
NH ₂ torsion	329	333	351	322	
OH wag	316	330	325	317	

coupled modes isolated. The deviations for both the NH_2 torsion and OH wagging decreased by 2 cm $^{-1}$. For trans-3-aminophenol, the use of this multilevel approach increased the deviation by 2 cm $^{-1}$. This may be in part due to how the predicted frequencies using B3LYP/aVTZ potentials were higher than those predicted with ccCA potentials.

The computed infrared (IR) spectra use the frequencies generated via VCIPSI-PT2 for potentials generated with ccCA and DFT (Figure 6). To show the efficacy of the VCIPSI-PT2 predictions, the generated spectra is compared to harmonic B3LYP/cc-pVTZ frequencies scaled by 1.0066 per the study by Merrick et al.¹⁷ The intensities for all frequencies are based on the harmonic calculation. Focusing on the area of the fingerprint region where the NH₂ torsion and OH wagging motion occur (200–400 cm⁻¹), the computed spectra shows peaks in the 200–300 cm⁻¹ range indicating torsional motion among the C atoms in the ring. For the NH₂ torsion and OH wagging motions for cis-3-aminophenol, the VCIPSI-PT2 frequencies with ccCA potentials were more closely aligned to experiment than both the scaled harmonic frequencies and VCIPSI-PT2 frequencies with potentials generated with B3LYP/aVTZ. The frequencies obtained via the ccCA

1096987x, 2024, 16, Downloaded from https://onlinelibrary.wiley.com/doi/10.1002/jcc.27333, Wiley Online Library on [10/11/2024]. See the Terms and Conditions (https://onlinelibrary.wiley.com/terms-and-conditions) on Wiley Online Library for rules of use; OA articles are governed by the applicable Creative Commons Licensea

FIGURE 6 Infrared spectra for cis-3-aminophenol (top) and trans-3-aminophenol (bottom) obtained with VCIPSI-PT2 frequencies with ccCA and B3LYP/aug-cc-pVTZ potentials as well as B3LYP/cc-pVTZ harmonic frequencies scaled by 1.0066. A Lorentz broadening of 20 cm⁻¹ was applied. IR intensities were normalized with the most intense peak in the fingerprint region. The experimental frequencies and relative intensities from Reference 9 are shown for comparison.



potentials with VCIPSI-PT2 combined with the IR intensities generated via VSCF yielded a more accurate representation of the spectra than the scaled harmonic frequencies and its respective IR intensities. Therefore, calculating the computed IR spectra with VCIPSI-PT2 frequencies with ccCA PESs and a full description of the mode-mode couplings would be more representative of the experimental IR spectra than using scaled harmonic frequencies.

4 | CONCLUSIONS

Overall, with ccCA potentials, the mean absolute deviation for calculated frequency from experiment was lower than with DFT potentials. Functional choice had a more significant effect on the predicted frequency than basis set for potentials generated with DFT. For diatomics, TPSS potentials tended to properly characterize molecules that exhibit covalent triple bonds and B3LYP potentials tended to yield lower absolute errors in frequency from experiment for polar molecules. This trend held with the small polyatomics and hydrocarbons. When considering timings, ccCA yielded lower deviations than CCSD(T,full)/aug-cc-pCV5Z with up to 99% CPU time savings for diatomic molecules.

For H_2O , CO_2 , and NH_3 , the predicted frequencies between potentials generated with ccCA and DFT yielded similar errors across all vibrations. DFT predicted the bending behaviors better than ccCA

whereas ccCA predicted the stretching behaviors better than DFT. The use of a curvilinear coordinate system yielded lower errors relative to using a standard Cartesian coordinate system as indicated by the deviations observed for H_2O and CO_2 .

For hydrocarbons, DFT characterized the C—H stretching behavior better than ccCA as the errors for DFT potentials were lower than for ccCA potentials for C—H stretching modes. Trends observed for all molecules examined indicate that B3LYP/aVTZ is the more favorable DFT method and basis set combination in terms of generating a PES for vibrational motion when coupled with VCIPSI-PT2 to compute frequencies. A multilevel approach that utilizes the single mode PECs with DFT and the coupled vibrational modes generated with ccCA yields lower absolute deviations from experiment than if only DFT were utilized, and therefore provides a framework for expanding to larger polyatomic systems and for molecular systems where one method generates PECs that yield lower deviations than another, as was the case with the hydrocarbons.

For aminophenol, the errors obtained with VCIPSI-PT2 were lower than those for scaled harmonics, indicating the success of utilizing this approach to characterize specific vibrations for polyatomic systems. The FASTVCI approach of only utilizing strongly coupled vibrational modes saves computational resources when generating potentials with electronic structure methods. B3LYP potentials serve as a good approximation for both the NH₂ torsional mode and OH wagging mode for both the cis-3-aminophenol and trans-3-aminophenol isomers. For cis-

3-aminophenol, the ccCA potentials yielded lower deviations for the NH₂ torsion where the opposite is true for trans-3-aminophenol.

Overall, *ab initio* composite strategies and in some cases DFT can be utilized for depicting vibrational behavior of small polyatomic molecules present in the interstellar medium and can be used in tandem with post-VSCF theory as a gauge for predicting anharmonic vibrations without the harmonic frequencies with frequency scaling factors applied and perturbative corrections.

ACKNOWLEDGMENTS

This material is based upon work supported by the National Science Foundation under Grant No. CHE-1900086 and Grant No. CHE-2154526. This work utilized computational facilities at the Institute for Cyber-Enabled Research (ICER) at Michigan State University. The MSU High School Honors Science Program (HSHSP) is acknowledged for the support of MAB. This submission is in honor of Elfi Kraka, and her many significant contributions to science as well as serving as an inspiration to so many of us in theoretical chemistry.

DATA AVAILABILITY STATEMENT

The data that supports the findings of this study are available in the supplementary material of this article.

ORCID

Prajay Patel https://orcid.org/0000-0002-6763-6295

Max Aksel Bowman https://orcid.org/0000-0002-1288-7687

Inga Ulusoy https://orcid.org/0000-0001-7294-4148

Angela K. Wilson https://orcid.org/0000-0001-9500-1628

REFERENCES

- [1] E. Pretsch, P. Buhlmann, M. Badertscher, in *Structure Determination of Organic Compounds* **2009**.
- [2] J. Bron, Can. J. Chem. 1975, 53, 3069.
- [3] J. M. Bakker, L. Mac Aleese, G. Meijer, G. von Helden, Phys. Rev. Lett. 2003, 91, 203003. https://doi.org/10.1103/PhysRevLett.91.203003
- [4] K. Kawaguchi, Handbook of Vibrational Spectroscopy, John Wiley & Sons, Ltd, Chichester, UK 2006.
- [5] A. Barth, Biochim. Biophys. Acta, Bioenerg. 2007, 1767, 1073. https://doi.org/10.1016/j.bbabio.2007.06.004
- [6] M. J. Almond, S. L. Jenkins, Encyclopedia of Inorganic and Bioinorganic Chemistry, John Wiley & Sons, Ltd, Chichester, UK 2011.
- [7] D. Cremer, E. Kraka, *Dalton Trans.* 2017, 46, 8323. https://doi.org/ 10.1039/C7DT00178A
- [8] M. Reichenbächer, J. Popp, in Challenges in Molecular Structure Determination 2012.
- [9] V. Yatsyna, D. J. Bakker, R. Feifel, A. M. Rijs, V. Zhaunerchyk, Phys. Chem. Chem. Phys. 2016, 18, 6275. https://doi.org/10.1039/ c5cp07426f
- [10] T. K. Roy, R. B. Gerber, Phys. Chem. Chem. Phys. 2013, 15, 9468. https://doi.org/10.1039/c3cp50739d
- [11] J. Bloino, A. Baiardi, M. Biczysko, Int. J. Quantum Chem. 2016, 116, 1543. https://doi.org/10.1002/qua.25188
- [12] M. McCutcheon, M. Freindorf, E. Kraka, J. Chem. Phys. 2022, 157, 014301. https://doi.org/10.1063/5.0094567
- [13] T. K. Roy, J. Phys. Chem. A 2022, 126, 608. https://doi.org/10.1021/acs.jpca.1c09989
- [14] W. Zou, M. Freindorf, V. Oliveira, Y. Tao, E. Kraka, Can. J. Chem. 2023, 101, 615. https://doi.org/10.1139/cjc-2022-0254

- [15] I. Respondek, D. M. Benoit, J. Chem. Phys. 2009, 131, 054109. https://doi.org/10.1063/1.3193708
- [16] A. P. Scott, L. Radom, J. Phys. Chem. 1996, 100, 16502. https://doi. org/10.1021/jp960976r
- [17] J. P. Merrick, D. Moran, L. Radom, J. Phys. Chem. A 2007, 111, 11683. https://doi.org/10.1021/jp073974n
- [18] M. L. Laury, S. E. Boesch, I. Haken, P. Sinha, R. A. Wheeler, A. K. Wilson, J. Comput. Chem. 2011, 32, 2339. https://doi.org/10.1002/jcc.21811
- [19] M. L. Laury, M. J. Carlson, A. K. Wilson, J. Comput. Chem. 2012, 33, 2380. https://doi.org/10.1002/jcc.23073
- [20] C. Latouche, F. Palazzetti, D. Skouteris, V. Barone, J. Chem. Theory Comput. 2014, 10, 4565. https://doi.org/10.1021/ct5006246
- [21] Q. Cheng, R. C. Fortenberry, N. J. DeYonker, J. Chem. Phys. 2017, 147, 234303. https://doi.org/10.1063/1.5006931
- [22] T. K. Roy, V. Kopysov, A. Pereverzev, J. Šebek, R. B. Gerber, O. V. Boyarkin, Phys. Chem. Chem. Phys. 2018, 20, 24894. https://doi.org/10.1039/C8CP03989E
- [23] P. A. Coles, R. I. Ovsyannikov, O. L. Polyansky, S. N. Yurchenko, J. Tennyson, J. Quantum Spectrosc. Radiat. Transf. 2018, 219, 199. https://doi.org/10.1016/j.jqsrt.2018.07.022
- [24] I. W. Bulik, M. J. Frisch, P. H. Vaccaro, J. Chem. Phys. 2017, 147, 044110. https://doi.org/10.1063/1.4995440
- [25] R. Knaanie, J. Šebek, M. Tsuge, N. Myllys, L. Khriachtchev, M. Räsänen, B. Albee, E. O. Potma, R. B. Gerber, J. Phys. Chem. A 2016, 120, 3380. https://doi.org/10.1021/acs.jpca.6b01604
- [26] D. M. Benoit, PVSCF | A Vibrational Theory Code. http://pvscf.org
- [27] G. A. Oyedepo, A. K. Wilson, J. Phys. Chem. A 2010, 114, 8806. https://doi.org/10.1021/jp1017949
- [28] S. A. Nedd, N. J. DeYonker, A. K. Wilson, P. Piecuch, M. S. Gordon, J. Chem. Phys. 2012, 136, 144109. https://doi.org/10.1063/1.3700801
- [29] N. J. DeYonker, T. R. Cundari, A. K. Wilson, J. Chem. Phys. 2006, 124, 114104. https://doi.org/10.1063/1.2173988
- [30] N. J. DeYonker, B. R. Wilson, A. W. Pierpont, T. R. Cundari, A. K. Wilson, Mol. Phys. 2009, 107, 1107. https://doi.org/10.1080/00268970902744359
- [31] P. Patel, T. R. L. Melin, S. C. North, A. K. Wilson, in Ab Initio Composite Methodologies: Their Significance for the Chemistry Community, Vol. 17, 2021
- [32] X. Xu, W. A. Goddard, J. Phys. Chem. A 2004, 108, 2305. https://doi. org/10.1021/jp035869t
- [33] D. Domin, D. M. Benoit, Chem. Phys. Chem. 2011, 12, 3383. https://doi.org/10.1002/cphc.201100499
- [34] Z. Konkoli, D. Cremer, Int. J. Quantum Chem. 1998, 67, 1. https://doi. org/10.1002/(SICI)1097-461X(1998)67:1<1::AID-QUA1>3.0.CO;2-Z
- [35] Z. Konkoli, J. A. Larsson, D. Cremer, Int. J. Quantum Chem. 1998, 67, 11. https://doi.org/10.1002/(SICI)1097-461X(1998)67:1<11::AID-QUA2>3.0.CO;2-1
- [36] Z. Konkoli, D. Cremer, Int. J. Quantum Chem. 1998, 67, 29. https://doi.org/10.1002/(SICI)1097-461X(1998)67:1<29::AID-QUA3>3.0. CO;2-0
- [37] Z. Konkoli, J. A. Larsson, D. Cremer, Int. J. Quantum Chem. 1998, 67,
 41. https://doi.org/10.1002/(SICI)1097-461X(1998)67:1<41::AID-QUA4>3.0.CO;2-Z
- [38] E. Kraka, M. Quintano, H. W. La Force, J. J. Antonio, M. Freindorf, J. Phys. Chem. A 2022, 126, 8781. https://doi.org/10.1021/acs.jpca. 2c05962
- [39] E. Kraka, W. Zou, Y. Tao, WIREs Comput. Mol. Sci. 2020, 10, 1. https://doi.org/10.1002/wcms.1480
- [40] M. Quintano, A. A. A. Delgado, R. T. Moura Jr., M. Freindorf, E. Kraka, Electron. Struct. 2022, 4, 044005. https://doi.org/10.1088/2516-1075/acaa7a
- [41] R. C. Fortenberry, X. Huang, A. Yachmenev, W. Thiel, T. J. Lee, Chem. Phys. Lett. 2013, 574, 1. https://doi.org/10.1016/j.cplett.2013. 03.078

- [42] R. C. Fortenberry, T. J. Lee, Vibr. Dynam. Mol. 2022, 1, 1.
- [43] B. R. Westbrook, J. P. Layfield, T. J. Lee, R. C. Fortenberry, *Electron. Struct.* 2022, 4, 045003. https://doi.org/10.1088/2516-1075/aca458
- [44] C. Zhang, J. Wang, A. M. Turner, J. H. Marks, S. Chandra, R. C. Fortenberry, R. I. Kaiser, Astrophys. J. 2023, 952, 132. https://doi.org/10.3847/1538-4357/acd451
- [45] S. Nickerson, N. Rangwala, S. W. J. Colgan, C. DeWitt, J. S. Monzon, X. Huang, K. Acharyya, M. N. Drozdovskaya, R. C. Fortenberry, E. Herbst, T. J. Lee, Astrophys. J. 2023, 945, 26. https://doi.org/10. 3847/1538-4357/aca6e8
- [46] J. M. Bowman, J. Chem. Phys. 1978, 68, 608. https://doi.org/10. 1063/1.435782
- [47] G. D. Carney, L. L. Sprandel, C. W. Kern, Advances in Chemical Physics, XXXVII, John Wiley & Sons, Inc., New York, 1978, p. 305.
- [48] R. B. Gerber, M. A. Ratner, Chem. Phys. Lett. 1979, 68, 195. https://doi.org/10.1016/0009-2614(79)80099-8
- [49] M. Cohen, S. Greita, R. P. McEarchran, Chem. Phys. Lett. 1979, 60, 445. https://doi.org/10.1016/0009-2614(79)80609-0
- [50] J. M. Bowman, Acc. Chem. Res. 1986, 19, 202. https://doi.org/10. 1021/ar00127a002
- [51] T. K. Roy, R. Sharma, R. B. Gerber, Phys. Chem. Chem. Phys. 2016, 18, 1607. https://doi.org/10.1039/c5cp05979h
- [52] J. M. Bowman, G. Czakó, B. Fu, Phys. Chem. Chem. Phys. 2011, 13, 8094. https://doi.org/10.1039/c0cp02722g
- [53] S. Seager, Proc. Natl. Acad. Sci. U. S. A. 2014, 111, 12634. https://doi. org/10.1073/pnas.1304213111
- [54] D. M. Benoit, B. Madebene, I. Ulusoy, L. Mancera, Y. Scribano, S. Chulkov, Beilstein J. Nanotechnol. 2011, 2, 427. https://doi.org/10.3762/bjnano.2.48
- [55] F. Neese, Wiley Interdiscip. Rev. Comput. Mol. Sci. 2012, 2, 73. https://doi.org/10.1002/wcms.81
- [56] F. Neese, Wiley Interdiscip. Rev. Comput. Mol. Sci. 2018. https://doi. org/10.1002/wcms.1327
- [57] G. Herzberg, Electronic Spectra and Electronic Structure of Polyatomic Molecules, Van Nostrand, New York 1966.
- [58] K. P. Huber, G. Herzberg, Molecular Spectra and Molecular Structure, Springer US. Boston. MA 1979.
- [59] T. Shimanouchi, in *Tables of Molecular Vibrational Frequencies*, Consolidated Vol. 1, Gaithersburg, MD 1972.
- [60] Y. Scribano, D. M. Lauvergnat, D. M. Benoit, J. Chem. Phys. 2010, 133, 094103. https://doi.org/10.1063/1.3476468
- [61] C. C. Marston, G. G. Balint-Kurti, J. Chem. Phys. 1989, 91, 3571. https://doi.org/10.1063/1.456888
- [62] G. G. Balint-Kurti, C. L. Ward, C. Clay Marston, Comput. Phys. Commun. 1991, 67, 285. https://doi.org/10.1016/0010-4655(91)90023-E

- [63] Y. Scribano, D. M. Benoit, Chem. Phys. Lett. 2008, 458, 384. https://doi.org/10.1016/j.cplett.2008.05.001
- [64] C. Lee, W. Yang, R. G. Parr, Phys. Rev. B 1988, 37, 785. https://doi. org/10.1103/PhysRevB.37.785
- [65] A. D. Becke, J. Chem. Phys. 1993, 98, 5648. https://doi.org/10.1063/ 1.464913
- [66] J. Tao, J. P. Perdew, V. N. Staroverov, G. E. Scuseria, Phys. Rev. Lett. 2003, 91, 146401. https://doi.org/10.1103/PhysRevLett.91.146401
- [67] S. F. Sousa, P. A. Fernandes, M. J. Ramos, J. Phys. Chem. A 2007, 111, 10439. https://doi.org/10.1021/jp0734474
- [68] T. H. Dunning Jr., J. Chem. Phys. 1989, 90, 1007. https://doi.org/10. 1063/1.456153
- [69] D. Feller, J. Chem. Phys. 1992, 96, 6104. https://doi.org/10.1063/1. 462652
- [70] A. Halkier, T. Helgaker, P. Jørgensen, W. Klopper, J. Olsen, Chem. Phys. Lett. 1999, 302, 437. https://doi.org/10.1016/S0009-2614(99) 00179-7
- [71] A. Halkier, W. Klopper, T. Helgaker, P. Jørgensen, J. Chem. Phys. 1999, 111, 4424. https://doi.org/10.1063/1.480036
- [72] K. A. Peterson, D. E. Woon, T. H. Dunning Jr., J. Chem. Phys. 1994, 100, 7410. https://doi.org/10.1063/1.466884
- [73] C. Schwartz, Phys. Rev. 1962, 126, 1015. https://doi.org/10.1103/ PhysRev.126.1015
- [74] C. Schwartz, Estimating Convergence Rates of Variational Calculations, Academic Press Inc, New York, NY 1963.
- [75] P. Patel, J. Wang, A. K. Wilson, J. Comput. Chem. 2020, 41, 171. https://doi.org/10.1002/jcc.26057
- [76] P. Patel, Z. Lu, M. G. Jafari, C. Hernández-Prieto, P. Zatsepin, D. J. Mindiola, D. M. Kaphan, M. Delferro, A. J. Kropf, C. Liu, J. Phys. Chem. C 2022, 126, 11949. https://doi.org/10.1021/acs.jpcc.2c02049
- [77] D. Feller, K. A. Peterson, D. A. Dixon, Annu. Rep. Comput. Chem. 2016. https://doi.org/10.1016/bs.arcc.2016.02.001

SUPPORTING INFORMATION

Additional supporting information can be found online in the Supporting Information section at the end of this article.

How to cite this article: P. Patel, J. Chung, M. A. Bowman, I. Ulusoy, A. K. Wilson, J. Comput. Chem. **2024**, 45(16), 1352. https://doi.org/10.1002/jcc.27333